Chapter 5
The *p*-version of the Finite Element Method

Barna Szabó[1], Alexander Düster[2] and Ernst Rank[2]

[1] *Washington University, St. Louis, MO, USA*
[2] *Lehrstuhl für Bauinformatik, Technische Universität München, Munich, Germany*

1 Introduction 119
2 Implementation 120
3 Convergence Characteristics 126
4 Performance Characteristics 131
5 Applications to Nonlinear Problems 133
6 Outlook 136
Acknowledgments 137
Notes 137
References 137
Further Reading 139

1 INTRODUCTION

The p-version of the finite element method (FEM) is presented as a method for obtaining approximate solutions to generalized formulations of the form

'Find $u \in X$ such that $\mathcal{B}(u, v) = \mathcal{F}(v)$ for all $v \in Y$' (1)

where u and v are scalar or vector functions in one, two, or three dimensions. In the displacement formulation of solid mechanics problems, for example, u is the displacement function, X is the space of admissible displacement functions, v is the virtual displacement function, Y is the space of admissible virtual displacement functions, $\mathcal{B}(u, v)$ is the virtual work of internal stresses, and $\mathcal{F}(v)$ is the virtual work of external forces.

More generally, u (resp. X) is called the *trial function* (resp. *trial space*) and v (resp. Y) is called the *test function* (resp. *test space*), $\mathcal{B}(u, v)$ is a bilinear form defined on $X \times Y$ and $\mathcal{F}(v)$ is a linear functional defined on Y. Associated with the spaces X and Y are the norms $\|\cdot\|_X$ and $\|\cdot\|_Y$. The definitive properties of bilinear forms and linear functionals are listed, for example, in Szabó and Babuška (1991), Schwab (1998), and Babuška and Strouboulis (2001).

The definitions for $\mathcal{B}(u, v)$, $\mathcal{F}(v)$, X, and Y depend on the choice of the generalized formulation and the boundary conditions. The solution domain will be denoted by Ω and the set of functions u that satisfy the condition $\mathcal{B}(u, u) \leq C < \infty$ on Ω will be called the *energy space* and denoted by $E(\Omega)$. The exact solution will be denoted by u_{EX}. The energy norm defined by

$$\|u\|_{E(\Omega)} := \sqrt{\tfrac{1}{2}\mathcal{B}(u, u)} \tag{2}$$

will be associated with the spaces $X \subset E(\Omega)$ and $Y \subset E(\Omega)$. It can be shown that this formulation is equivalent to the minimization of the potential energy functional defined by

$$\Pi(u) := \tfrac{1}{2}\mathcal{B}(u, u) - \mathcal{F}(u) \tag{3}$$

The exact solution u_{EX} of equation (1) is the minimizer of $\Pi(u)$ on the space $X \subset E(\Omega)$.

In the finite element method, finite dimensional subspaces $S \subset X$ and $V \subset Y$ are constructed. These spaces are characterized by the finite element mesh, the polynomial degrees assigned to the elements, and the mapping

Encyclopedia of Computational Mechanics, Edited by Erwin Stein, René de Borst and Thomas J.R. Hughes. Volume 1: *Fundamentals*. ISBN: 0-470-84699-2.

functions. Details are given in Section 2. An approximation to u_{EX}, denoted by u_{FE}, is obtained by solving the finite dimensional problem:

'Find $u_{FE} \in S$ such that $\mathcal{B}(u_{FE}, v) = \mathcal{F}(v)$ for all $v \in V$' (4)

The dimension of V is the number of degrees of freedom, denoted by N.

A key theorem states that the finite element solution u_{FE} minimizes the error in energy norm

$$\|u_{EX} - u_{FE}\|_{E(\Omega)} = \min_{u \in S} \|u_{EX} - u\|_{E(\Omega)} \tag{5}$$

It is seen that the error in energy norm depends on the choice of S. Proper choice of S depends on the regularity of u_{EX}, the objectives of computation, and the desired level of precision.

Another important theorem establishes the following relationship between the error measured in energy norm and the potential energy:

$$\|u_{EX} - u_{FE}\|^2_{E(\Omega)} = \Pi(u_{FE}) - \Pi(u_{EX}) \tag{6}$$

Proofs are available in Szabó and Babuška (1991). In the p-version, this theorem is used in a posteriori estimation of error in energy norm.

The data of interest are functionals of u_{EX}: $\Psi_1(u_{EX})$, $\Psi_2(u_{EX}), \ldots$ approximated by $\Psi_1(u_{FE})$, $\Psi_2(u_{FE}), \ldots$. An important objective of finite element computations is to establish that the relative errors in the data of interest are small. Therefore, it is necessary to show that

$$|\Psi_i(u_{EX}) - \Psi_i(u_{FE})| \leq \tau_i |\Psi_i(u_{EX})| \qquad i = 1, 2, \ldots \tag{7}$$

where τ_i are prescribed tolerances. Of course, $\Psi_i(u_{EX})$ is generally unknown; however, $\Psi_i(u_{EX})$ is known to be independent of the choice of the space S. Therefore, if we compute a sequence of finite element solutions corresponding to a hierarchic sequence of finite element spaces $S_1 \subset S_2 \subset S_3 \cdots$ then $\Psi_i(u_{FE}) \to \Psi_i(u_{EX})$. The limiting value of $\Psi_i(u_{FE})$ and hence τ_i can be estimated. The p-version of the finite element method is well suited for the creation of hierarchic finite element spaces and hence the estimation and control of errors in terms of the data of interest.

2 IMPLEMENTATION

From the theoretical point of view, the quality of approximation is completely determined by the finite element space characterized by the finite element mesh Δ, the polynomial degrees of elements $\mathbf{p}$, and the mapping functions $\mathbf{Q}$ (see Section 2.4). Specifically, the finite element space S is a set of functions constructed from polynomials defined on standard elements that are mapped onto the elements of the finite element mesh, subject to the appropriate continuity requirements to ensure that it is a subset of the energy space

$$S := \left\{ u | u \in E(\Omega), u(Q^k) \in \mathcal{S}^{p_k},\ k = 1, 2, \ldots, M(\Delta) \right\}$$

where Q^k is the mapping function for the kth element, $\mathcal{S}^{p_k}$ is the polynomial space of degree p_k associated with the kth element, and $M(\Delta)$ is the number of elements. Different sets of basis functions, called *shape functions*, can be chosen to define the same finite element space; however, there are some important considerations:

1. For a wide range of mapping parameters, the round-off error accumulation with respect to increasing polynomial degree should be as small as possible. (Ideally, the element-level stiffness matrices should be perfectly diagonal, but it is neither necessary nor practical to choose the shape functions in that way in two and three dimensions.)
2. The shape functions should permit computation of the stiffness matrices and load vectors as efficiently as possible.
3. The shape functions should permit efficient enforcement of exact and minimal continuity.
4. The choice of the shape functions affects the performance of iterative solution procedures. For large problems, this can be the dominant consideration.

The first three points suggest that shape functions should be constructed from polynomial functions that have certain orthogonality properties; should be *hierarchic*, that is, the set of shape functions of polynomial degree p should be in the set of shape functions of polynomial degree $p + 1$, and the number of shape functions that do not vanish at vertices, edges, and faces should be the smallest possible. Some of the shape functions used in various implementations of the p-version are described in the following.

2.1 Hierarchic shape functions for one-dimensional problems

The *classical* finite element *nodal basis functions* in one dimension on the *standard element* $\Omega_{\text{st}} = (-1, 1)$ are illustrated on the left-hand side of Figure 1.

The standard shape functions are defined by the set of Lagrange polynomials

$$N_i^p(\xi) = \prod_{j=1, j \neq i}^{p+1} \frac{\xi - \xi_j}{\xi_i - \xi_j} \tag{8}$$

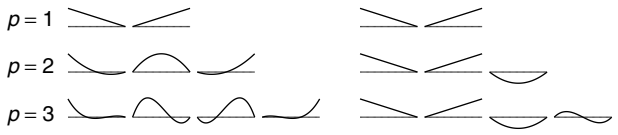

Figure 1. Set of one-dimensional standard and hierarchic shape functions for $p = 1, 2, 3$. (Reproduced by permission of John Wiley & Sons, Ltd from A. Düster, H. Bröker and E. Rank, *Int. J. Numer. Meth. Eng.*, **52**, 673–703 (2001).)

The points ξ_j where

$$N_i^p(\xi_j) = \delta_{ij} = \begin{cases} 0 & \text{if } i \neq j \\ 1 & \text{if } i = j \end{cases} \tag{9}$$

are called *nodes*. There are certain advantages in selecting the nodes to be the Gauss–Lobatto points as done in the spectral element method, which is also addressed in this encyclopedia (see **Chapter 3, Volume 3**). This approach has been modified to suit the p-version of the finite element method in Melenk, Gerdes and Schwab (2001). Note that the sum of all Lagrange polynomials for a given polynomial degree p equals unity:

$$\sum_{i=1}^{p+1} N_i^p(\xi) = 1 \tag{10}$$

Every function that can be represented as a linear combination of this standard basis can be represented also by the set of hierarchic basis functions (see the right-hand side of Figure 1). A principal difference between the two bases is that in the hierarchic case all lower-order shape functions are contained in the higher-order basis. The set of one-dimensional hierarchic shape functions, introduced by Szabó and Babuška (1991), is given by

$$N_1(\xi) = \tfrac{1}{2}(1 - \xi) \tag{11}$$

$$N_2(\xi) = \tfrac{1}{2}(1 + \xi) \tag{12}$$

$$N_i(\xi) = \phi_{i-1}(\xi), \quad i = 3, 4, \ldots, p + 1 \tag{13}$$

with

$$\phi_j(\xi) = \sqrt{\frac{2j-1}{2}} \int_{-1}^{\xi} L_{j-1}(x)\,\mathrm{d}x = \frac{1}{\sqrt{4j-2}}(L_j(\xi) - L_{j-2}(\xi)), \quad j = 2, 3, \ldots \tag{14}$$

where $L_j(\xi)$ are the Legendre polynomials. The first two shape functions $N_1(\xi)$, $N_2(\xi)$ are called *nodal shape functions* or *nodal modes*. Because

$$N_i(-1) = N_i(1) = 0, \quad i \geq 3 \tag{15}$$

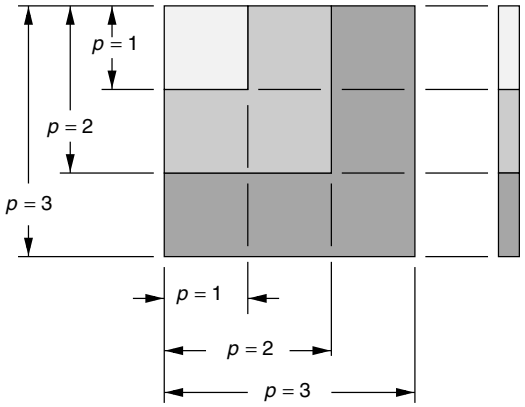

Figure 2. Hierarchic structure of stiffness matrix and load vector with $p = 3$. (Reproduced by permission of John Wiley & Sons, Ltd from E. Stein (Editor), *Error-controlled Adaptive Finite Elements in Solid Mechanics*, 263–307 (2002).)

the functions $N_i(\xi), i = 3, 4, \ldots$ are called *internal shape functions*, *internal modes*, or *bubble modes*. The orthogonality property of Legendre polynomials implies

$$\int_{-1}^{1} \frac{\mathrm{d}N_i}{\mathrm{d}\xi} \frac{\mathrm{d}N_j}{\mathrm{d}\xi}\,\mathrm{d}\xi = \delta_{ij}, \quad i \geq 3 \quad \text{and} \quad j \geq 1 \quad \text{or} \quad i \geq 1 \quad \text{and} \quad j \geq 3 \tag{16}$$

If equations are ordered in such a way that all linear modes are numbered from 1 to n_1, all quadratic modes are numbered from $n_1 + 1$ to n_2 and so on, stiffness matrices corresponding to polynomial order 1 to $p - 1$ are submatrices of the stiffness matrix corresponding to polynomial order p. Figure 2 depicts the structure of a stiffness matrix and a load vector corresponding to polynomial degree of $p = 3$ schematically.

2.2 Hierarchic shape functions for quadrilaterals

The standard quadrilateral finite element is shown in Figure 4. Two types of standard polynomial spaces, the *trunk space* $\mathcal{S}_{\mathrm{ts}}^{p_\xi, p_\eta}(\Omega_{\mathrm{st}}^{\mathrm{q}})$ and the *tensor product space* $\mathcal{S}_{\mathrm{ps}}^{p_\xi, p_\eta}(\Omega_{\mathrm{st}}^{\mathrm{q}})$, are discussed in the following. The *tensor product space* $\mathcal{S}_{\mathrm{ps}}^{p_\xi, p_\eta}(\Omega_{\mathrm{st}}^{\mathrm{q}})$ consists of all polynomials on $\Omega_{\mathrm{st}}^{\mathrm{q}} = [(-1, 1) \times (-1, 1)]$ spanned by the set of monomials $\xi^i \eta^j$ where $i = 0, 1, \ldots, p_\xi$, $j = 0, 1, \ldots, p_\eta$, whereas the trunk space $\mathcal{S}_{\mathrm{ts}}^{p_\xi, p_\eta}(\Omega_{\mathrm{st}}^{\mathrm{q}})$ on $\Omega_{\mathrm{st}}^{\mathrm{q}} = [(-1, 1) \times (-1, 1)]$ is spanned by the set of all monomials

- $\xi^i \eta^j$ with $i = 0, \ldots, p_\xi$, $j = 0, \ldots, p_\eta$, $i + j = 0, \ldots, \max\{p_\xi, p_\eta\}$
- $\xi\eta$ for $p_\xi = p_\eta = 1$
- $\xi^{p_\xi}\eta$ for $p_\xi \geq 2$
- $\xi\eta^{p_\eta}$ for $p_\eta \geq 2$.

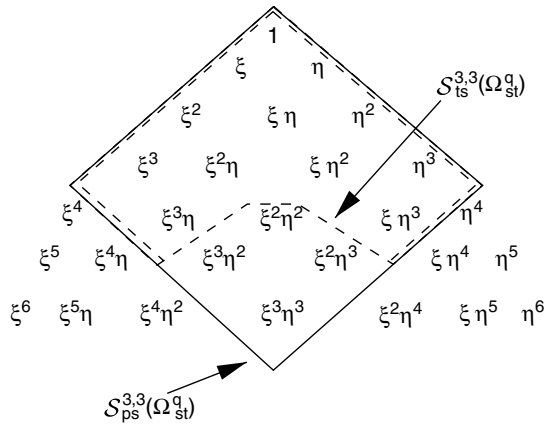

Figure 3. The trunk space $\mathcal{S}^{3,3}_{ts}(\Omega^q_{st})$ and the tensor product space $\mathcal{S}^{3,3}_{ps}(\Omega^q_{st})$. (Reproduced by permission of John Wiley & Sons, Ltd from E. Stein (Editor), *Error-controlled Adaptive Finite Elements in Solid Mechanics*, 263–307 (2002).)

The difference between the two standard polynomial spaces can be readily visualized when considering the spanning sets in Pascal's triangle. The set of monomials for $p_\xi = p_\eta = 3$ for both the trunk and the tensor product space is shown in Figure 3. All monomials inside the dashed line span the trunk space $\mathcal{S}^{3,3}_{ts}(\Omega^q_{st})$, whereas the monomials bordered by the solid line are essential for the tensor product space $\mathcal{S}^{3,3}_{ps}(\Omega^q_{st})$.

Two-dimensional shape functions can be classified into three groups: nodal, edge, and internal shape functions. Using the numbering convention shown in Figure 4, these shape functions are described in the following.

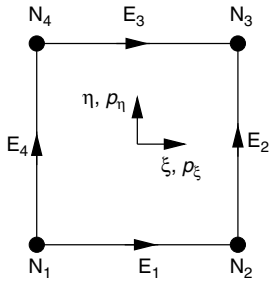

Figure 4. Standard quadrilateral element Ω^q_{st}: definition of nodes, edges, and polynomial degree.

1. **Nodal or vertex modes:** The nodal modes

$$N^{N_i}_{1,1}(\xi, \eta) = \tfrac{1}{4}(1 + \xi_i \xi)(1 + \eta_i \eta), \quad i = 1, \ldots, 4 \tag{17}$$

are the standard bilinear shape functions, well known from the isoparametric four-noded quadrilateral element. (ξ_i, η_i) denote the local coordinates of the ith node.

2. **Edge or side modes:** These modes are defined separately for each individual edge, they vanish at all other edges. The corresponding modes for edge E_1 read:

$$N^{E_1}_{i,1}(\xi, \eta) = \tfrac{1}{2}(1 - \eta)\phi_i(\xi), \quad i \geq 2 \tag{18}$$

3. **Internal modes:** The internal modes

$$N^{\text{int}}_{i,j}(\xi, \eta) = \phi_i(\xi)\phi_j(\eta), \quad i, j \geq 2 \tag{19}$$

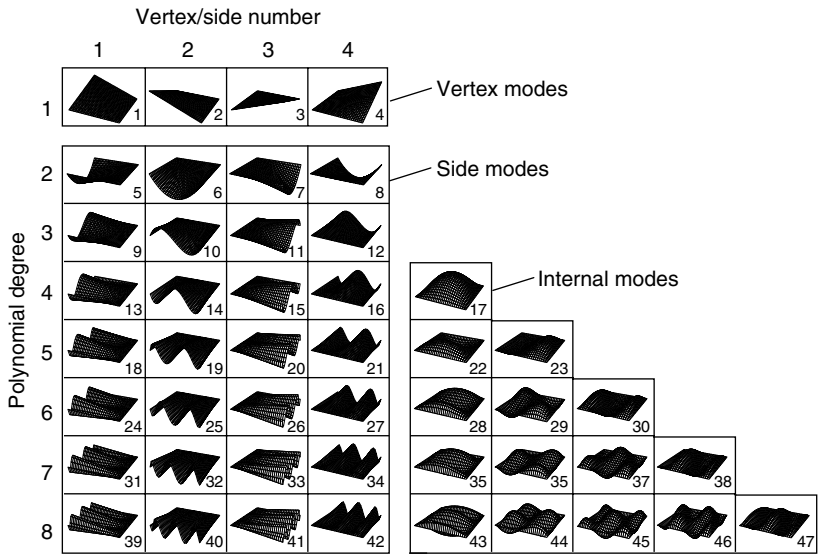

Figure 5. Hierarchic shape functions for quadrilateral elements. Trunk space, $p = 1$ to $p = 8$. (From *Finite Element Analysis*; B. Szabó and I. Babuška; Copyright (1991) John Wiley & Sons, Inc. This material is used by permission of John Wiley & Sons, Inc.)

are purely local and vanish at the edges of the quadrilateral element.

As already indicated, the indices i, j of the shape functions denote the polynomial degrees in the local directions ξ, η. In Figure 5, all hierarchic shape functions that span the trunk space are plotted up to order $p = 8$.

2.3 Hierarchic shape functions for hexahedrals

The implementation of high-order finite elements in three dimensions can be based on a hexahedral element formulation (see Figure 6), again using the hierarchic shape functions introduced by Szabó and Babuška (1991). High-order hexahedral elements are suited for solid, 'thick' structures and for thin-walled structures alike. In the case of plate- or shell-like structures, one local variable can be identified to correspond with the thickness direction and it is possible to choose the polynomial degree in the thickness direction differently from those in the in-plane direction; see Düster, Bröker and Rank (2001). Generalizing the two-dimensional concept, three-dimensional shape functions can be classified into four groups:

1. **Nodal or vertex modes:** The nodal modes

$$N^{\mathrm{N}_i}_{1,1,1}(\xi,\eta,\zeta) = \frac{1}{8}(1+\xi_i\xi)(1+\eta_i\eta)(1+\zeta_i\zeta), \quad i = 1,\ldots,8 \tag{20}$$

   are the standard trilinear shape functions, well known from the isoparametric eight-noded brick element. (ξ_i, η_i, ζ_i) are the local coordinates of the ith node.
2. **Edge modes:** These modes are defined separately for each edge. If we consider, for example, edge E_1 (see Figure 6), the corresponding edge modes read:

$$N^{\mathrm{E}_1}_{i,1,1}(\xi,\eta,\zeta) = \tfrac{1}{4}(1-\eta)(1-\zeta)\phi_i(\xi), \quad i \geq 2 \tag{21}$$

3. **Face modes:** These modes are defined separately for each individual face. If we consider, for example, face F_1, the corresponding face modes read:

$$N^{\mathrm{F}_1}_{i,j,1}(\xi,\eta,\zeta) = \tfrac{1}{2}(1-\zeta)\phi_i(\xi)\phi_j(\eta), \quad i,j \geq 2 \tag{22}$$

4. **Internal modes:** The internal modes

$$N^{\mathrm{int}}_{i,j,k}(\xi,\eta,\zeta) = \phi_i(\xi)\phi_j(\eta)\phi_k(\zeta), \quad i,j,k \geq 2 \tag{23}$$

   are purely local and vanish at the faces of the hexahedral element.

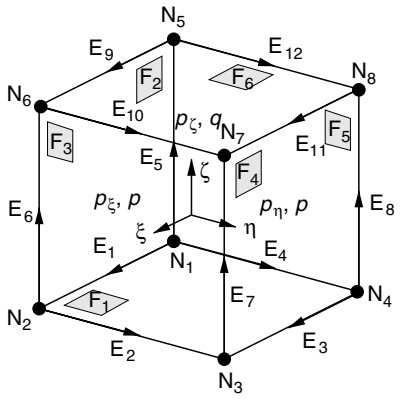

Figure 6. Standard hexahedral element $\Omega^{\mathrm{h}}_{\mathrm{st}}$: definition of nodes, edges, faces, and polynomial degree.

The indices i, j, k of the shape functions denote the polynomial degrees in the local directions ξ, η, ζ.

Three different types of trial spaces can be readily defined: the *trunk space* $\mathcal{S}^{p_\xi,p_\eta,p_\zeta}_{\mathrm{ts}}(\Omega^{\mathrm{h}}_{\mathrm{st}})$, the *tensor product space* $\mathcal{S}^{p_\xi,p_\eta,p_\zeta}_{\mathrm{ps}}(\Omega^{\mathrm{h}}_{\mathrm{st}})$, and an *anisotropic tensor product space* $\mathcal{S}^{p,p,q}(\Omega^{\mathrm{h}}_{\mathrm{st}})$. A detailed description of these trial spaces can be found in Szabó and Babuška (1991). The polynomial degree for the trial spaces $\mathcal{S}^{p_\xi,p_\eta,p_\zeta}_{\mathrm{ts}}(\Omega^{\mathrm{h}}_{\mathrm{st}})$ and $\mathcal{S}^{p_\xi,p_\eta,p_\zeta}_{\mathrm{ps}}(\Omega^{\mathrm{h}}_{\mathrm{st}})$ can be varied separately in each local direction (see Figure 6). Differences between the trunk and product spaces occur in the face modes and internal modes only. For explanation, we first consider the face modes, for example, the modes for face 1. Indices i, j denote the polynomial degrees of the face modes in ξ and η direction, respectively.

Face modes (face $\mathbf{F_1}$): $N^{\mathrm{F}_1}_{i,j,1}(\xi,\eta,\zeta) = 1/2(1-\zeta)\phi_i(\xi)\,\phi_j(\eta)$

trunk space	**tensor product space**
$i = 2,\ldots,p_\xi - 2$	$i = 2,\ldots,p_\xi$
$j = 2,\ldots,p_\eta - 2$	$j = 2,\ldots,p_\eta$
$i + j = 4,\ldots,\max\{p_\xi, p_\eta\}$	

The definition of the set of internal modes is very similar. Indices i, j, k now denote the polynomial degrees in the three local directions ξ, η, and ζ.

Internal modes: $N^{\mathrm{int}}_{i,j,k}(\xi,\eta,\zeta) = \phi_i(\xi)\phi_j(\eta)\phi_k(\zeta)$

trunk space	**tensor product space**
$i = 2,\ldots,p_\xi - 4$	$i = 2,\ldots,p_\xi$
$j = 2,\ldots,p_\eta - 4$	$j = 2,\ldots,p_\eta$
$k = 2,\ldots,p_\zeta - 4$	$k = 2,\ldots,p_\zeta$
$i + j + k = 6,\ldots,\max\{p_\xi, p_\eta, p_\zeta\}$	

The space $\mathcal{S}^{p,p,q}(\Omega^{\mathrm{h}}_{\mathrm{st}})$ defines an anisotropic set of shape functions determined by two polynomial degrees p and q (see Figure 6). All shape functions of higher order in ξ and η direction are associated with the polynomial degree p. These shape functions correspond to the edges 1, 2, 3, 4, 9, 10, 11, 12, to the faces 1 and 6 and to all internal modes. Shape functions for faces 1 and 6 are equal to those of the trunk space $\mathcal{S}^{p_\xi,p_\eta,p_\zeta}_{\mathrm{ts}}(\Omega^{\mathrm{h}}_{\mathrm{st}})$ with $p_\xi = p_\eta = p$. q defines the degree of all shape functions of higher order in ζ-direction that are associated with the edges 5, 6, 7, 8, with the faces 2, 3, 4, 5, and with all internal modes. The modes corresponding to the faces 2, 3, 4, 5, are equal to those of the tensor product space $\mathcal{S}^{p_\xi,p_\eta,p_\zeta}_{\mathrm{ps}}(\Omega^{\mathrm{h}}_{\mathrm{st}})$ with $p = p_\xi = p_\eta$ and $q = p_\zeta$. Considering a polynomial degree $p = q = p_\xi = p_\eta = p_\zeta$, one observes that the number of internal modes of $\mathcal{S}^{p,p,q}(\Omega^{\mathrm{h}}_{\mathrm{st}})$ is larger than that of the trunk space $\mathcal{S}^{p_\xi,p_\eta,p_\zeta}_{\mathrm{ts}}(\Omega^{\mathrm{h}}_{\mathrm{st}})$ but smaller than that of the tensor product space $\mathcal{S}^{p_\xi,p_\eta,p_\zeta}_{\mathrm{ps}}(\Omega^{\mathrm{h}}_{\mathrm{st}})$.

Owing to the built-in anisotropic behavior of the trial space $\mathcal{S}^{p,p,q}(\Omega^{\mathrm{h}}_{\mathrm{st}})$, it is important to consider the orientation of the local coordinates of a hexahedral element. Figure 7 shows how hexahedral elements should be oriented when three-dimensional, thin-walled structures are discretized. The local coordinate ζ of the hexahedral element corresponds to the thickness direction. If the orientation of all elements is the same then it is possible to construct discretizations where the polynomial degree for the in-plane and thickness directions of thin-walled structures can be treated differently.

2.4 Mapping

In low-order finite element analysis (FEA), the most frequently used mapping technique for the geometric description of the domain of computation is the application of isoparametric elements where the standard shape functions are used for the geometric description of elements. The same shape functions are used for the approximation of the unknown solution and for the shape of the elements. Using elements of order $p = 1$ or $p = 2$, the boundary of the domain is approximated by a polygonal or by a piecewise parabolic curve, respectively. As the mesh is refined, the boundary of the domain is approximated more and more accurately. When using the p-version, on the other hand, the mesh remains fixed. It is therefore important to model the geometry of the structure accurately with the fixed number of elements. This calls for a method that is able to describe complex geometries using only a few elements. Gordon and Hall (1973a,b) proposed the *blending function method* that is usually applied when describing curved boundaries of p-version finite elements; see, for example, Szabó and Babuška (1991) and Düster, Bröker and Rank (2001). After introducing blending function mapping, an example will compare polynomial interpolation versus exact blending mapping and demonstrate the necessity of a precise description of geometry.

2.4.1 The blending function method

Consider a quadrilateral element as shown in Figure 8 where edge E_2 is assumed to be part of a curved boundary. The shape of edge E_2 is assumed to be defined by a parametric function $\mathbf{E}_2 = [E_{2x}(\eta), E_{2y}(\eta)]^{\mathrm{T}}$, where η is the local coordinate of the element. The transformation of the local coordinates $\boldsymbol{\xi} = [\xi, \eta]^{\mathrm{T}}$ into the global coordinates $\mathbf{x} = [x, y]^{\mathrm{T}} = \mathbf{Q}^e = [Q^e_x(\xi, \eta), Q^e_y(\xi, \eta)]^{\mathrm{T}}$ can be formulated by the two functions

$$
\begin{aligned}
x = Q^e_x(\xi, \eta) &= \sum_{i=1}^{4} N^{\mathrm{N}_i}_{1,1}(\xi, \eta) X_i \\
&\quad + \left(E_{2x}(\eta) - \left(\frac{1-\eta}{2} X_2 + \frac{1+\eta}{2} X_3 \right) \right) \frac{1+\xi}{2} \\
y = Q^e_y(\xi, \eta) &= \sum_{i=1}^{4} N^{\mathrm{N}_i}_{1,1}(\xi, \eta) Y_i \\
&\quad + \left(E_{2y}(\eta) - \left(\frac{1-\eta}{2} Y_2 + \frac{1+\eta}{2} Y_3 \right) \right) \frac{1+\xi}{2}
\end{aligned}
\tag{24}
$$

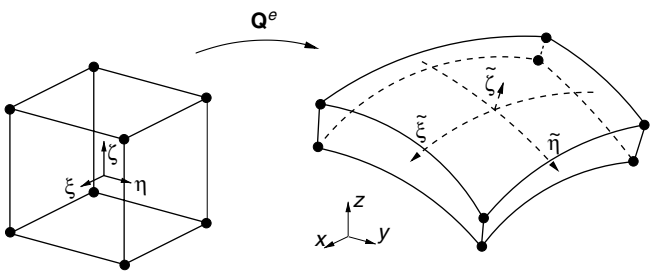

Figure 7. Modelling thin-walled structures with hexahedral elements.

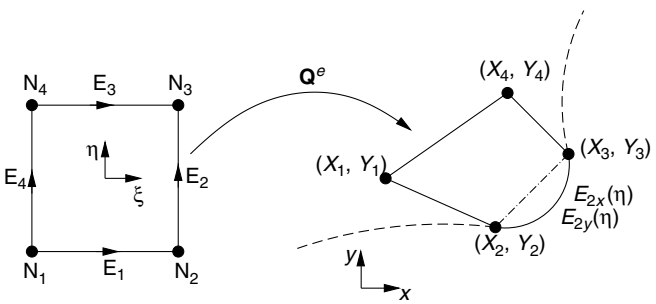

Figure 8. Blending function method for quadrilateral elements.

where the first term corresponds to the standard bilinear mapping that is familiar from the isoparametric concept for quadrilateral elements with $p = 1$. The second term takes the curved edge E_2 into account. Therefore, the bilinear mapping is augmented by the blended difference between the curve $\mathbf{E}_2 = [E_{2x}(\eta), E_{2y}(\eta)]^T$ and the straight line connecting the nodes N_2 and N_3. The blending term $(1 + \xi)/2$ ensures that the opposite edge E_4 – where $(1 + \xi)/2 = 0$ – is not affected by the curvilinear description of edge E_2.

If a quadrilateral in which all edges are curved is to be considered, the blending function method can be expanded such that the mapping reads

$$\begin{aligned} x = Q_x^e(\xi, \eta) &= \frac{1}{2}(1-\eta)E_{1x}(\xi) + \frac{1}{2}(1+\xi)E_{2x}(\eta) \\ &+ \frac{1}{2}(1+\eta)E_{3x}(\xi) + \frac{1}{2}(1-\xi)E_{4x}(\eta) \\ &- \sum_{i=1}^{4} N_{1,1}^{N_i}(\xi, \eta)X_i \\ y = Q_y^e(\xi, \eta) &= \frac{1}{2}(1-\eta)E_{1y}(\xi) + \frac{1}{2}(1+\xi)E_{2y}(\eta) \\ &+ \frac{1}{2}(1+\eta)E_{3y}(\xi) + \frac{1}{2}(1-\xi)E_{4y}(\eta) \\ &- \sum_{i=1}^{4} N_{1,1}^{N_i}(\xi, \eta)Y_i \end{aligned} \tag{25}$$

where

$$\begin{aligned} &E_{ix}(\xi),\ E_{iy}(\xi), \quad \text{for} \quad i = 1, 3 \\ &E_{ix}(\eta),\ E_{iy}(\eta), \quad \text{for} \quad i = 2, 4 \end{aligned} \tag{26}$$

are parametric functions describing the shape of the edges $\mathbf{E}_i$, $i = 1, 2, 3, 4$. Therefore the blending function method allows arbitrary parametric descriptions of the edges of elements.

2.4.2 *Accuracy of mapping versus polynomial interpolation*

The following numerical example demonstrates the importance of accurate representation of geometry when a p-extension is to be applied in order to find a finite element approximation. A quarter of a linear elastic square plate with a central circular hole and unit thickness (1 mm) is loaded by a traction $T_n = 100$ MPa (see Figure 9). The dimensions are chosen to be $b = h = 100$ mm and $R = 10$ mm. At the lower and right side of the plate, symmetry conditions are imposed. The isotropic linear elastic material behavior is characterized by Young's modulus $E = 206\,900$ MPa, Poisson's ratio $\nu = 0.29$, and plane

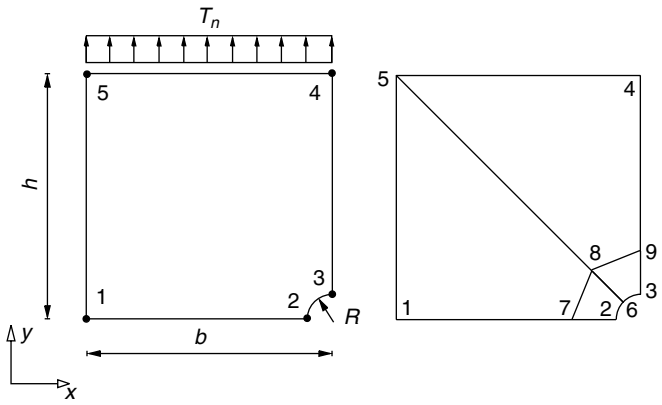

Figure 9. Perforated square plate under uniform tension.

stress assumptions. The strain energy of the plate – obtained by an 'overkill' finite element approximation – amounts to 247.521396 Nmm. The plate is discretized by four quadrilateral elements and the circle with radius $R = 10$ mm is represented by applying

1. **exact blending:** that is, the exact parametric description of a circle is applied;
2. **parabolic description:** two parabolas are used to interpolate the circle with a corresponding relative error $(|R - \tilde{R}|/R)100(\%) < 0.0725(\%)$, where $\tilde{R}$ denotes the radius of the interpolated circle.

A p-extension based on the tensor product space $\mathcal{S}_{ps}^{p,p}(\Omega_{st}^q)$, $p = 1, \ldots, 8$ is performed and the relative error in energy norm for both the exact blending and the parabolic boundary interpolation is plotted versus the degrees of freedom on a log–log scale in Figure 10. Owing to the smoothness of the exact solution of the problem, the p-extension in conjunction with the exact blending shows exponential rate of convergence (see equation (29) in Section 3.2). In the case of the parabolic boundary interpolation, the convergence rate of the p-extension deteriorates for $p \geq 3$ and the strain energy finally converges to an incorrect value. Consider the stresses, for instance, stress component σ_{yy} at point 2; we observe that the p-extension with $p = 1, \ldots, 20$ and exact blending converges rapidly while the stress obtained with parabolic boundary interpolation diverges (see Figure 11).

Although the relative error of the parabolic geometric interpolation seems to be very small, it has a strong influence on the accuracy of the p-extension. The strain energy of the approximation converges to an incorrect value and the stress component σ_{yy} at point 2 even diverges. The reason for this is that an artificial stress singularity is introduced. Considering the first derivatives at the interelement node 6, and at symmetry nodes 2

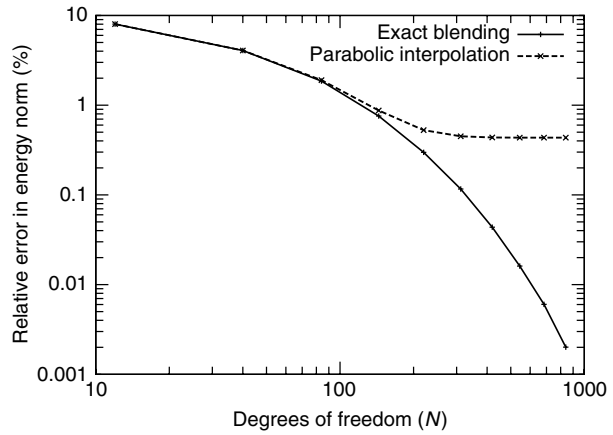

Figure 10. Influence of the blending on the relative error in energy norm.

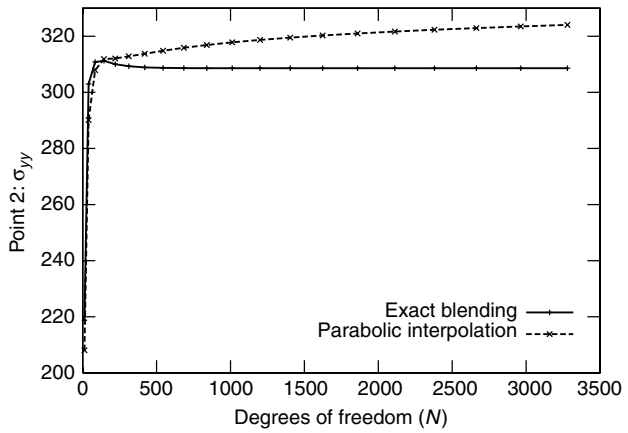

Figure 11. Influence of the blending on the stress component σ_{yy} at point 2.

and 3, discontinuities are observed. They lead to stress singularities similar to stress concentrations at corners. One way of avoiding these stress singularities is to use the exact blending or to apply the so-called quasi-regional mapping described in Királyfalvi and Szabó (1997). The idea of the quasi-regional mapping is to combine the blending function method with a polynomial interpolation of geometry, using optimal collocation points; see Chen and Babuska (1995, 1996). An example of the effectiveness of this kind of mapping is given in connection with a geometrically nonlinear problem in Section 5.2. A detailed comparison of exact and polynomial blending is given by Bröker (2001).

3 CONVERGENCE CHARACTERISTICS

In this section, some key theoretical results that establish relationships between the error in energy norm and the number of degrees of freedom associated with hierarchic sequences of finite element spaces: $S_1 \subset S_2 \subset \cdots$ are presented.

In the early implementations of the finite element method, the polynomial degrees were restricted to $p = 1$ or $p = 2$ only. Finite element spaces were enlarged by mesh refinement, that is, by reducing the diameter of the largest element, denoted by h. Subsequently, this limitation was removed, allowing enlargement of finite element spaces by increasing the polynomial degree of elements, denoted by p, while keeping the mesh fixed. To distinguish between the two approaches, the terms 'h-version' and 'p-version' gained currency. We will consider three strategies for constructing finite element spaces:

(a) h-Extension: The polynomial degree of elements is fixed, typically at some low number, such as $p = 1$ or $p = 2$, and the number of elements is increased such that h is progressively reduced.
(b) p-Extension: The mesh is fixed and the polynomial degree of elements is increased.
(c) hp-Extension: The mesh is refined and the polynomial degrees of elements are concurrently increased.

A fourth strategy, not considered here, introduces basis functions, other than the mapped polynomial basis functions described in Section 2, to represent some local characteristics of the exact solution. This is variously known as the *space enrichment method*, *partition of unity method*, and *meshless method*.

It is of considerable practical interest to know how the first space S_1 should be constructed and when and how h-extension, p-extension, or hp-extension should be used. The underlying principles and practical considerations are summarized in the following.

3.1 Classification

It is useful to establish a simple classification for the exact solution based on a priori information available concerning its regularity. The exact solution, denoted by u_{EX} in the following, may be a scalar function or a vector function.

Category A: u_{EX} is analytic everywhere on the solution domain including the boundaries. By definition, a function is analytic in a point if it can be expanded into a Taylor series about that point. The solution is in category A also when analytical continuation is applicable.

Category B: u_{EX} is analytic everywhere on the solution domain including the boundaries, with the exception of a finite number of points (or in 3D, a finite number of points and edges). The locations where the

exact solution is not analytic are called *singular points* or *singular edges*. The great majority of practical problems in solid mechanics belong in this category. Problems in category B are characterized by *piecewise analytic data*, that is, the domain is bounded by piecewise analytic functions and/or the boundary conditions are piecewise analytic.

Category C: u_{EX} is neither in category A nor in category B.

At corner singularities and at intersections of material interfaces in two-dimensional problems, the exact solution typically can be written in the form

$$\mathbf{u}_{EX} = \sum_{i=1}^{\infty} A_i r^{\lambda_i} \mathbf{F}_i(\theta), \quad r < \rho, \quad \lambda_{\min} > 0 \tag{27}$$

where r, θ are polar coordinates centered on the singular point, A_i, λ_i are real numbers, $\mathbf{F}_i$ is an analytic (or piecewise analytic) vector function, and ρ is the radius of convergence. Additional details can be found in Grisvard (1985). This is known as an asymptotic expansion of the solution in the neighborhood of a singular point. Analogous expressions can be written for one and three dimensions with $\lambda_{\min} > 1 - d/2$ where d is the number of spatial dimensions. The minimum value of λ_i corresponding to a nonzero coefficient A_i characterizes the regularity (also called 'smoothness') of the exact solution. In the following section, the key theorems concerning the asymptotic rates of convergence of the various extension processes are summarized.

3.2 A priori estimates

A priori estimates of the rates of convergence are available for solutions in categories A, B, and C. Convergence is either algebraic or exponential. The algebraic estimate is of the form

$$\|\mathbf{u}_{EX} - \mathbf{u}_{FE}\|_{E(\Omega)} \leq \frac{k}{N^{\beta}} \tag{28}$$

and the exponential estimate is of the form

$$\|\mathbf{u}_{EX} - \mathbf{u}_{FE}\|_{E(\Omega)} \leq \frac{k}{\exp(\gamma N^{\theta})} \tag{29}$$

These estimates should be understood to mean that there exists some positive constant k, and a positive constant β (resp. γ and θ) that depend on $\mathbf{u}_{EX}$, such that the error will be bounded by the algebraic (resp. exponential) estimate as the number of degrees of freedom N is increased. These estimates are sharp for sufficiently large N.

The asymptotic rates of convergence for two-dimensional problems are summarized in Table 1 and for three-dimensional problems in Table 2. In these tables, p (resp. λ) represents the minimum polynomial degree assigned to the elements of a finite element mesh (resp. $\lambda_{\min}$ in equation (27)) (see **Chapter 4, this Volume**).

3.3 The choice of finite element spaces

The theoretical results described in Section 3.2 provide an important conceptual framework for the construction of finite element spaces (see **Chapter 3, this Volume**).

3.3.1 Problems in category A

Referring to Tables 1 and 2, it is seen that for problems in category A, exponential rates of convergence are possible through p- and hp-extensions. These convergence rates can be realized provided that all singular points lie on element vertices and edges. For both the p- and hp-extensions, the optimal mesh consists of the smallest number of elements required to partition the solution domain into triangular

Table 1. Asymptotic rates of convergence in two dimensions.

Category	Type of extension		
	h	*p*	*hp*
A	Algebraic $\beta = p/2$	Exponential $\theta \geq 1/2$	Exponential $\theta \geq 1/2$
B	Algebraic Note 1 $\beta = (1/2)\min(p, \lambda)$	Algebraic $\beta = \lambda$	Exponential $\theta \geq 1/3$
C	Algebraic $\beta > 0$	Algebraic $\beta > 0$	Note 2

Note 1: Uniform or quasi-uniform mesh refinement is assumed. In the case of optimal mesh refinement, $\beta_{\max} = p/2$.
Note 2: When $\mathbf{u}_{EX}$ has a recognizable structure, then it is possible to achieve faster than algebraic rates of convergence with *hp*-adaptive methods.

Table 2. Asymptotic rates of convergence in three dimensions.

Category	Type of extension		
	h	*p*	*hp*
A	Algebraic $\beta = p/3$	Exponential $\theta \geq 1/3$	Exponential $\theta \geq 1/3$
B	Note 3		Exponential $\theta \geq 1/5$
C	Algebraic $\beta > 0$	Algebraic $\beta > 0$	Note 2

Note 3: In three dimensions, $\mathbf{u}_{EX}$ cannot be characterized by a single parameter. Nevertheless, the rate of p-convergence is at least twice the rate of h-convergence.

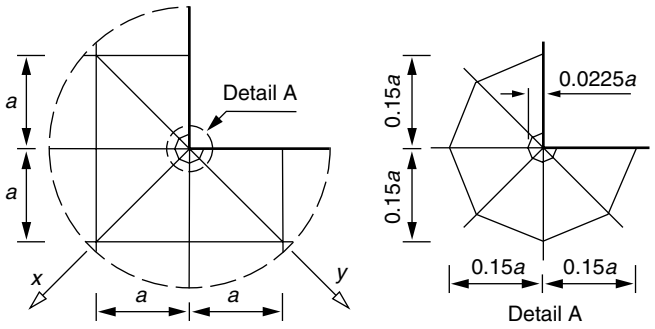

Figure 12. Example of a geometric mesh (detail).

and quadrilateral elements in two dimensions; tetrahedral, pentahedral, and hexahedral elements in three dimensions.

When h-extensions are used, the optimal rate of convergence in 2D is algebraic with $\beta = p/2$. The optimal mesh grading depends on both p and the exact solution.

3.3.2 Problems in category B

When the exact solution can be written in the form of equation (27), there is an optimal design of the discretization in the neighborhood of the singular point. The finite elements should be laid out so that the sizes of elements decrease in geometric progression toward the singular point (located at $x = 0$) and the polynomial degrees of elements increase away from the singular point. The optimal grading is $q = (\sqrt{2} - 1)^2 \approx 0.17$ that is independent of $\lambda_{\min}$. In practice, $q = 0.15$ is used. These are called *geometric meshes*. An example of a geometric mesh in two dimensions is given in Figure 12.

The ideal distribution of polynomial degrees is that the lowest polynomial degree is associated with the smallest element and the polynomial degrees increase linearly away from the singular points. This is because the errors in the vicinity of singular points depend primarily on the size of elements, whereas errors associated with elements farther from singular points, where the solution is smooth, depend mainly on the polynomial degree of elements. In practice, uniform p-distribution is used, which yields very nearly optimal results in the sense that convergence is exponential, and the work penalty associated with using uniform polynomial degree distribution is not substantial.

3.4 A simple 1D model problem

In this section, we will consider an axially loaded linear elastic bar as depicted in Figure 13.

Although the solution of the underlying simple model problem (30)–(32) can be stated in a closed form, it

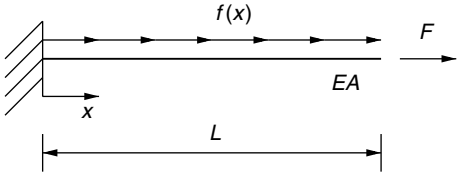

Figure 13. Linear elastic bar.

is worth studying because it implies many of the features that also appear in more complex models. Furthermore, the general concept of the p-version can be readily represented when considering the simple one-dimensional model problem. A tutorial program for a one-dimensional h-, p-, and hp-version of the finite element method, where the following problems can be investigated in detail, has been implemented in Maple [1]. The solution $u(x)$(length) of the ordinary differential equation (30) describes the displacement of the bar in x-direction, being loaded by a traction $f(x)$(force/length) and a load F(force). E(force/length^2) denotes Young's modulus, A(length^2) the cross-sectional area, and L(length) the length of the bar.

$$-(EAu'(x))' = f(x) \quad \text{on} \quad \Omega = [x|0 \le x \le L] \tag{30}$$

$$u = 0 \quad \text{at} \quad x = 0 \tag{31}$$

$$EAu' = F \quad \text{at} \quad x = L \tag{32}$$

For the sake of simplicity, it is assumed that the displacement $u(x)$ and strain $\varepsilon = \mathrm{d}u/\mathrm{d}x$ are small and that the bar exhibits a linear elastic stress–strain relationship, that is, $\sigma = E\varepsilon$ with σ being uniformly distributed over the cross-sectional area A. Equation (31) defines a Dirichlet boundary condition at $x = 0$ and equation (32), a Neumann boundary condition at $x = L$. For a detailed study of this model problem, see Szabó and Babuška (1991). The variational or weak formulation of the model problem (30)–(32), which is the basis for a finite element approximation can be stated as follows:

Find $u \in X$ satisfying (homogeneous) Dirichlet boundary conditions, such that

$$\mathcal{B}(u, v) = \mathcal{F}(v) \quad \text{for all} \quad v \in Y \tag{33}$$

where

$$\mathcal{B}(u, v) = \int_0^L EAu'v' \,\mathrm{d}x$$

$$\text{and} \quad \mathcal{F}(v) = \int_0^L fv \,\mathrm{d}x + Fv(L) \tag{34}$$

3.4.1 A numerical example with a smooth solution

Figure 13 shows an elastic bar where it is assumed that $EA = L = 1$, $f(x) = -\sin(8x)$ and $F = 0$. The p-version discretizations consist of one element with $p = 1, 2, 3, \ldots, 8$, whereas the h-version is based on a uniformly refined mesh with up to eight linear ($p = 1$) elements.

First, we will consider the p-version discretization. The exact solution $u_{EX}(x) = -(1/64)\sin(8x) + (1/8)\cos(8)x$ of the problem (33)–(34) is approximated by a polynomial expression on the basis of the hierarchic shape functions (11)–(13)

$$u_{FE}(\xi) = N_1(\xi)U_1 + N_2(\xi)U_2 + \sum_{p=2}^{p_{\max}} N_{p+1}(\xi)a_{p+1} \quad (35)$$

where $p_{\max} = 8$. U_1 and U_2 denote the nodal displacements, whereas $a_3, \ldots, a_9$ are coefficients determining the higher-order terms of the approximation $u_{FE}(\xi)$. Owing to the orthonormality property (16) of the higher-order shape functions, the element stiffness matrix, $K^e_{ij} = (2/L) \int_{-1}^{1} EA(\mathrm{d}N_i(\xi)/\mathrm{d}\xi)(\mathrm{d}N_j(\xi)/\mathrm{d}\xi)\,\mathrm{d}\xi$, $i, j = 1, 2, 3, \ldots, 9$, is almost perfectly diagonal:

$$\mathbf{K}^e = \begin{bmatrix} 1 & -1 & 0 & 0 & \cdots & 0 \\ -1 & 1 & 0 & 0 & \cdots & 0 \\ 0 & 0 & 2 & 0 & \cdots & 0 \\ 0 & 0 & 0 & 2 & \cdots & 0 \\ \vdots & \vdots & \vdots & \vdots & \ddots & \vdots \\ 0 & 0 & 0 & 0 & \cdots & 2 \end{bmatrix} \quad (36)$$

Computing the element load vector, $F^e_i = (L/2) \int_{-1}^{1} N_i(\xi) f(x(\xi))\,\mathrm{d}\xi$, $i = 1, 2, 3, \ldots, 9$, one finds

$$\mathbf{F}^e = [-0.1095, -0.0336, -0.0269, -0.0714, 0.0811, 0.0433, -0.0230, -0.0073, 0.0026]^{\mathrm{T}} \quad (37)$$

Because of the homogenous Dirichlet boundary condition ($u(0) = u_{FE}(0) = 0 \rightarrow U_1 = 0$), the solution of the resulting diagonal equation system is trivial in this case. In Figure 14, the p-version approximation $u_{FE}(x)$ for $p = 1, 2, 3, \ldots, 8$ is plotted together with the exact solution of the problem. For a first comparison of the accuracy, the same problem is solved by applying the h-version with $p = 1$ based on a uniformly refined mesh with decreasing element size $h_i = 1/i$, $i = 1, \ldots, 8$. Again, the approximation and the exact solution is drawn (see Figure 15).

In Figure 16, the relative error in energy norm

$$(e_r)_{E(\Omega)} = \frac{\|u_{EX} - u_{FE}\|_{E(\Omega)}}{\|u_{EX}\|_{E(\Omega)}} \quad (38)$$

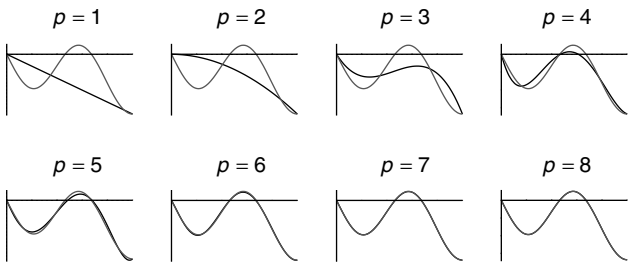

Figure 14. p-version solution $u_{FE}(x)$ based on one element with $p = 1, 2, 3, \ldots, 8$. A color version of this image is available at http://www.mrw.interscience.wiley.com/ecm

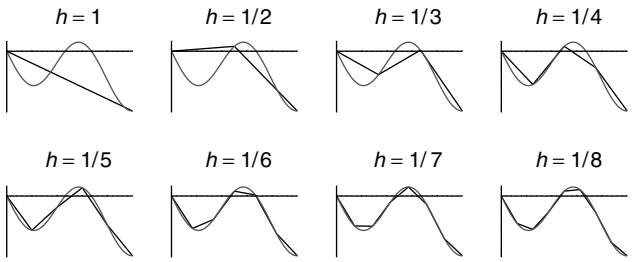

Figure 15. h-version solution $u_{FE}(x)$ based on a uniform refined mesh with $p = 1$. A color version of this image is available at http://www.mrw.interscience.wiley.com/ecm

is plotted versus the number of degrees of freedom in a double logarithmic style. By the classification given in Section 3.2, this problem is in category A, where the p-version exhibits exponential convergence (29), whereas the asymptotic rate of convergence of the h-extension is algebraic (28). For category A problems in one dimension, the parameter β in equation (28) is $\beta = p$. Since in this case $p = 1$, the asymptotic rate of convergence is 1, as shown in Figure 16.

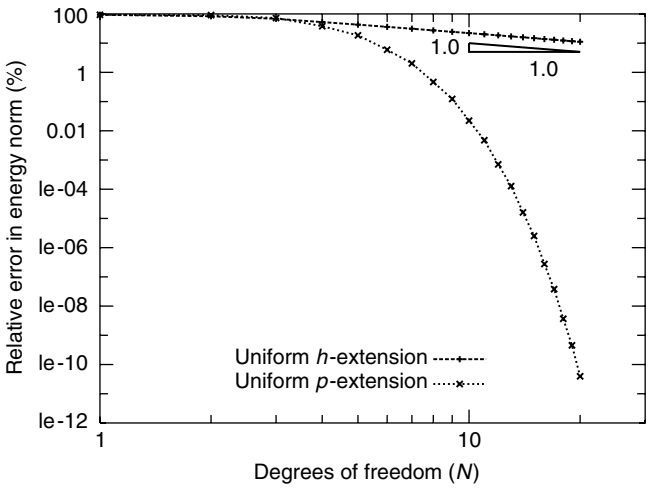

Figure 16. Comparison of the h- and p-version: relative error in energy norm.

3.4.2 A numerical example with a nonsmooth solution

In the following example, we will again consider the weak formulation (33)–(34) of the model problem (30)–(32) where $f(x)$ is now chosen such that the exact solution is nonsmooth. We define $f(x) = \lambda(\lambda - 1)x^{\lambda-2}$, $F = 0$ and $EA = L = 1$, resulting in an exact solution $u_{EX} = -x^{\lambda} + \lambda x$, where λ is the parameter controlling the smoothness of the solution. If $\lambda < 1.0$, then the first derivative of the exact solution will exhibit a singularity at $x = 0$ and the given problem will be in category B. Note that $\lambda > 1/2$ is a necessary condition for obtaining a finite strain energy of the exact solution. For the following numerical example, λ is chosen to be 0.65.

In Figure 17, the relative error in energy norm (38) is plotted versus the number of degrees of freedom on a log–log scale. p-Extension was performed on one element with $p = 1, \ldots, 50$, whereas the h-extension was performed on meshes with equal sized elements $h = 1, \ldots, 1/50$ with $p = 1$. Since the given problem is in category B, both extensions show algebraic convergence of type (28). The asymptotic rate of convergence of the h-extension is given by

$$\beta = \min\left(p, \lambda - \tfrac{1}{2}\right) = 0.15 \tag{39}$$

and can be clearly observed in Figure 17. The rate of convergence of the uniform p-extension is twice the rate of the uniform h-extension. This is due to the fact that the point where the exact solution exhibits singular behavior coincides with a node.

When combining mesh refinement with an increase in polynomial degree, exponential convergence in energy norm (29) can be achieved with an hp-extension, even when the exact solution u_{EX} has singularities. The mesh is refined towards the singular points by geometric progression using the common factor $q = 0.15$. The location of the nodal points X_i is given by

$$X_i = \begin{cases} 0 & \text{for } i = 0 \\ Lq^{n_{\text{el}}-i} & \text{for } i = 1, 2, \ldots, n_{\text{el}} \end{cases} \tag{40}$$

A polynomial degree $p_{\min} = 1$ is assigned to the element at the singularity, and increases linearly away from the singular point to the maximum degree

$$p_{\max} = (2\lambda - 1)(n_{\text{el}} - 1) \tag{41}$$

where λ denotes the smoothness of the solution and n_{el}, the total number of elements of the corresponding mesh. With this hp-extension, one obtains an exponential convergence in energy norm as shown in Figure 18 (hp-version, $q = 0.15$, $\lambda = 0.65$). Using about 100 degrees of freedom, the error is by several orders of magnitude smaller than that of a uniform p-version with one element or of a uniform h-version with $p = 1$.

Figure 18 also shows the results of uniform p-extensions obtained on geometrically refined meshes with $q = 0.15$. These extensions are performed on meshes with $n_{\text{el}} = 4, 8, 12, 16, 20, 24$ elements with p being uniformly increased from 1 to 8. In the preasymptotic range, the p-extension on fixed, geometrically graded meshes shows an exponential convergence rate. In the asymptotic range, the exponential convergence decreases to an algebraic rate, being limited by the smoothness λ of the exact solution. If proper meshes are used, that is, if the number of refinements corresponds to the polynomial degree, then any required accuracy is readily obtained.

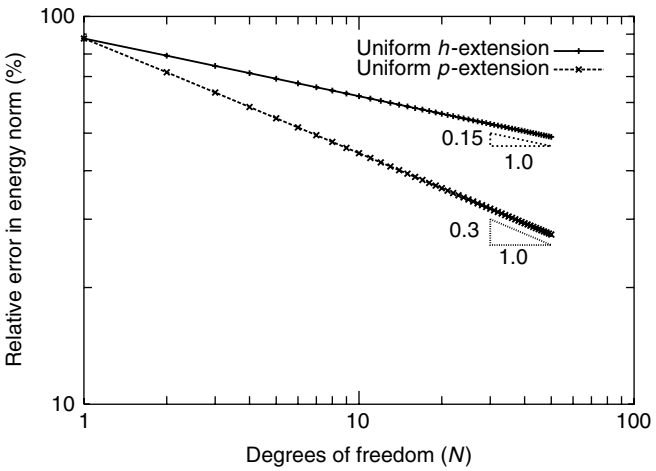

Figure 17. Comparison of the h- and p-version: relative error in energy norm.

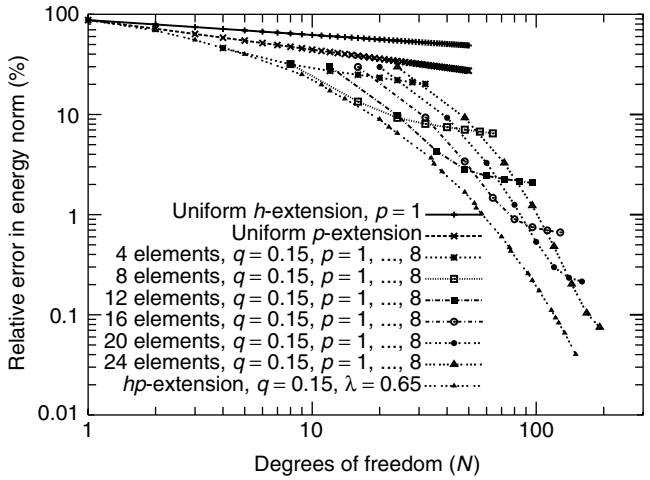

Figure 18. Comparison of the h-, p-, and hp-version: relative error in energy norm.

3.5 Model problem: The L-shaped domain

In order to illustrate the convergence characteristics of the *h*-, *p*-, and *hp*-extensions for category B problems, we consider an L-shaped domain in two-dimensional elasticity, under the assumption of plane strain conditions using Poisson's ratio 0.3. The reentrant edges are stress-free. In the *xy* coordinates system shown in Figure 12, the exact solution (up to rigid body displacement and rotation terms) corresponding to the first term of the asymptotic expansion is

$$u_x = \frac{A_1}{2G} r^{\lambda_1} [(\kappa - Q_1(\lambda_1 + 1)) \cos \lambda_1 \theta - \lambda_1 \cos(\lambda_1 - 2)\theta] \tag{42}$$

$$u_y = \frac{A_1}{2G} r^{\lambda_1} [(\kappa + Q_1(\lambda_1 + 1)) \sin \lambda_1 \theta + \lambda_1 \sin(\lambda_1 - 2)\theta] \tag{43}$$

where G is the shear modulus, $\lambda_1 = 0.544483737$, $Q_1 = 0.543075579$, and $\kappa = 1.8$. The coefficient A_1 is called a *generalized stress intensity factor*. Details are available in Szabó and Babuška (1991). The corresponding stress components are

$$\sigma_x = A_1 \lambda_1 r^{\lambda_1 - 1} [(2 - Q_1(\lambda_1 + 1)) \cos(\lambda_1 - 1)\theta - (\lambda_1 - 1) \cos(\lambda_1 - 3)\theta] \tag{44}$$

$$\sigma_y = A_1 \lambda_1 r^{\lambda_1 - 1} [(2 + Q_1(\lambda_1 + 1)) \cos(\lambda_1 - 1)\theta + (\lambda_1 - 1) \cos(\lambda_1 - 3)\theta] \tag{45}$$

$$\tau_{xy} = A_1 \lambda_1 r^{\lambda_1 - 1} [(\lambda_1 - 1) \sin(\lambda_1 - 3)\theta + Q_1(\lambda_1 + 1) \sin(\lambda_1 - 1)\theta] \tag{46}$$

This model problem is representative of an important class of problems. The reentrant edges are stress-free, the other boundaries are loaded by the tractions that correspond to the exact stress distribution given by equations (44) to (46). Since the exact solution is known, it is possible to compute the exact value of the potential energy from the definition of $\Pi(u_{EX})$ given by equation (3) and using $\mathcal{B}(u_{EX}, u_{EX}) = \mathcal{F}(u_{EX})$ from equation (1):

$$\Pi(u_{EX}) = -\frac{1}{2} \oint [u_x(\sigma_x n_x + \tau_{xy} n_y) + u_y(\tau_{xy} n_x + \sigma_y n_y)] \, ds = -4.15454423 \frac{A_1 a^{2\lambda_1}}{E} \tag{47}$$

where n_x, n_y are the components of the unit normal to the boundary and a is the dimension shown in the inset in Figure 12. The convergence paths for *h*- and *p*-extensions are shown in Figure 19.

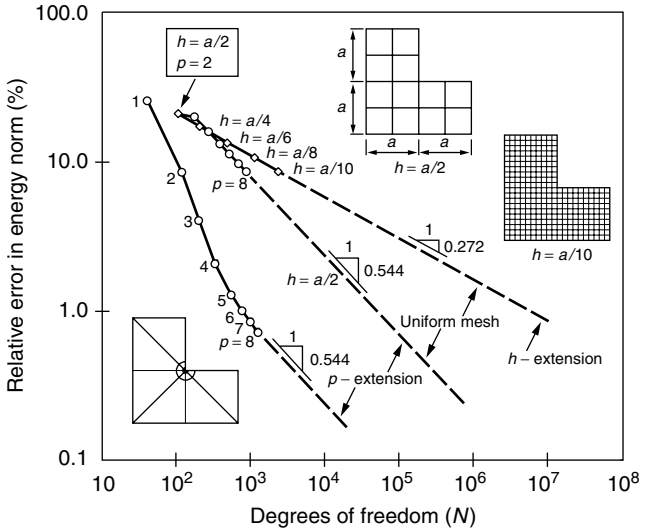

Figure 19. Convergence paths for the L-shaped domain. (From *Finite-Element Analysis*; B. Szabó and I. Babuška; Copyright (1991) John Wiley & Sons, Inc. This material is used by permission of John Wiley & Sons, Inc.)

It is seen that the asymptotic rates of convergence are exactly as predicted by the estimate (28). However, when *p*-extension is used on a geometric mesh, the preasymptotic rate is exponential or nearly so. This can be explained by observing that the geometric mesh shown in Figure 12 is overrefined for low polynomial degrees, hence the dominant source of the error is that part of the domain where the exact solution is smooth and hence the rate of convergence is exponential, as predicted by the estimate (29). Convergence slows to the algebraic rate for small errors, where the dominant source of error is the immediate vicinity of the singular point.

The error estimate frequently used in conjunction with *p*-extensions is based on the equation (6) and the use of Richardson extrapolation utilizing the a priori estimate (28). When *hp*-adaptivity has to be considered, local-based error estimators have to be applied; see, for example, Ainsworth and Oden (2000) and Melenk and Wohlmuth (2001). By definition, the effectivity index θ is the estimated error divided by the true error. The estimated and true errors and the effectivity indices are shown in Table 3. The parameter β is the same as that in equation (28).

4 PERFORMANCE CHARACTERISTICS

We have seen in Figure 19 that for a fixed accuracy (say 1%) there is a very substantial reduction in the number of degrees of freedom when *p*-extension is performed on properly designed meshes. From a practical point of view, the important consideration is the cost of computational

Table 3. L-shaped domain. Geometric mesh, 18 elements, trunk space. Plane strain, $\nu = 0.3$. Estimated and true relative errors in energy norm and effectivity index θ.

p	N	$\frac{\Pi(\mathbf{u}_{FE})E}{A_1^2 a^{2\lambda_1} t_z}$	β		$(e_r)_E$ (%)		θ
			Est.'d	True	Est.'d	True	
1	41	−3.886332	—	—	25.42	25.41	1.00
2	119	−4.124867	1.03	1.03	8.44	8.46	1.00
3	209	−4.148121	1.37	1.36	3.91	3.93	0.99
4	335	−4.152651	1.33	1.30	2.09	2.14	0.98
5	497	−4.153636	0.99	0.94	1.42	1.48	0.96
6	695	−4.153975	0.78	0.68	1.09	1.17	0.93
7	929	−4.154139	0.69	0.60	0.89	0.99	0.89
8	1199	−4.154238	0.69	0.56	0.75	0.86	0.87
∞	∞	−4.154470		0.54		0	

resources rather than the number of degrees of freedom. The proper basis for comparing the performance characteristics of various implementations of the h- and p-versions of the finite-element method is the cost of computation. The cost has to be evaluated with respect to representative model problems, such as the L-shaped domain problem discussed in Section 3.5, given specific goals of computation, the required accuracies, and the requirement that *a reasonably close estimate of the accuracy of the computed data of interest* be provided. It is essential that comparisons of performance include a verification process, that is, a process by which it is ascertained that the relative errors in the data of interest are within prespecified error tolerances. Verification is understood in relation to the exact solution of the mathematical model, not in relation to some physical reality that the model is supposed to represent. The consequences of wrong engineering decisions based on erroneous information usually far outweigh the costs of verification.

Comparative performance characteristics of the h- and p-versions were first addressed in Babuska and Scapolla (1987) and Babuska and Elman (1989) through analyses of computational complexity and theoretical error estimates as well as computer timing of specific benchmark problems. The main conclusions are summarized as follows:

1. Only for the uncommon cases of very low accuracy requirements and very irregular exact solutions are low-order elements preferable to high-order elements. High-order elements typically require smaller computational effort for the same level of accuracy.
2. High-order elements are more robust than low-order elements. This point is discussed further in Section 4.1 below.
3. The most effective error control procedures combine proper mesh design coupled with progressive increase in p. For details, we refer to Rank and Babuska (1987), Babuska and Suri (1990), and Rank (1992).
4. Accuracies normally required in engineering computation can be achieved with elements of degree 8 or less for most practical problems.
5. Computation of a sequence of solutions corresponding to a hierarchic sequence of finite element spaces $S_1 \subset S_2 \subset \cdots$ provides for simple and effective estimation and control of error for all data of interest, based on various types of extrapolation and extraction procedures; see, for example, Szabó and Babuska (1988), Szabó (1990), and Yosibash and Szabó (1994).

As a general rule, for problems in categories A and B (defined in Section 3.1), which include the vast majority of practical problems in solid mechanics, p-extension on properly designed meshes is the most efficient general solution strategy. The performance of p-extensions in solving problems on category C is discussed in Section 5.1.1.

In the p-version, the elemental matrices are large and their computation is time-consuming. On the other hand, these operations lend themselves to parallel computation; see, for example, Rank *et al.* (2001). Furthermore, it has been shown that a substantial reduction in time can be achieved if special integration techniques are used (see Nübel, Düster and Rank, 2001), or if the hierarchic structure is sacrificed (see Melenk, Gerdes and Schwab, 2001).

4.1 Robustness

A numerical method is said to be robust when it performs well for a broad class of admissible data. For example, in the displacement formulation of linear elasticity, letting Poisson's ratio ν approach $1/2$ causes the volumetric strain (div $\mathbf{u}$) to approach zero. This introduces constraints among the variables, effectively reducing the number of degrees of freedom, and hence causing the rate of convergence in energy norm to decrease, in some cases, very substantially. This phenomenon is called *locking*. Locking also causes problems in the recovery of the first stress invariant from the finite element solution. A similar situation exists when the thickness approaches zero in plate models based on the Reissner formulation. For a precise definition of robustness, we refer to Babuska and Suri (1992). It was shown in Vogelius (1983) that the rate of convergence in p-extensions is not influenced by $\nu \to 1/2$ on straight sided triangles. It is also known that the h-version using straight triangles does not exhibit locking, provided that $p \geq 4$. For curvilinear elements, the rate of p-convergence is slower, and for the h-version the locking problem is generally much more severe. Although the p-version is affected by membrane locking, in the range of typical plate and shell thicknesses that occur in practical engineering problems, locking effects are generally not substantial. For

an investigation of membrane locking in cylindrical shells, we refer to Pitkäranta (1992).

4.2 Example

The following example is representative of shell intersection problems. Specifically, the intersection of two cylindrical shells is considered. Referring to Figure 20, the outside radius of shell A is $R_A = 140$ mm, the outside radius of shell B is $R_B = 70$ mm. The wall thickness of shell A (resp. shell B) is $t_A = 8.5$ mm; (resp. $t_B = 7.5$ mm). The axes of the shells intersect at $\alpha = 65°$. The length of shell A is 800 mm, the length of shell B, measured from the point of intersection of the axes of the shells, is 300 mm. The modulus of elasticity is $E = 72.4$ MPa, Poisson's ratio is $\nu = 0.3$.

The intersection of the outer surfaces of the shells is filleted by a 'rolling ball fillet', that is, the fillet surface is generated as if rolling a sphere of radius $r_f = 10.0$ mm along the intersection line. The mesh consists of 34 hexahedral elements. The shell intersection region, comprised of 16 elements, is the darker region shown in Figure 20. The complement is the shell region. Quasi-regional mapping utilizing 6×6 collocation points per curved face was employed.

The inside surface is loaded by a pressure $\bar{p}$. In order to establish equilibrium, a normal traction T_n is applied on the surface S_B, which is the surface of intersection between shell B and a plane perpendicular to its axis:

$$T_n = \frac{\bar{p}(R_B - t_B)^2}{t_B(2R_B - t_B)} \tag{48}$$

The yz plane is a plane of symmetry. The other surfaces are traction-free. Appropriate rigid body constraints were imposed in order to prevent motion parallel to the plane of symmetry.

The objective is to estimate the magnitude of the maximal von Mises stress to within 5% relative error. In the shell intersection region, the solution varies substantially over distances comparable to the thickness. Therefore, dimensional reduction cannot be justified for this region. Fully three-dimensional elements, that is, elements based on the trunk spaces $\mathcal{S}_{\text{ts}}^{p,p,p}(\Omega_{\text{st}}^{\text{h}})$ with $p = 1, 2, \ldots, 8$ were used in the shell intersection region, whereas the anisotropic spaces $\mathcal{S}_{\text{ts}}^{p,p,q}(\Omega_{\text{st}}^{\text{h}})$ were used in the shell region. The computations were performed with StressCheck [2].

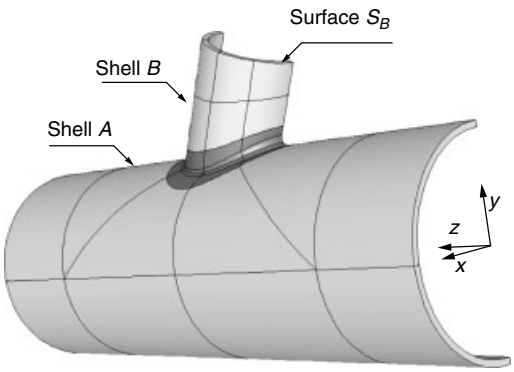

Figure 20. Example: Shell intersection problem. The darker region, comprised of 16 elements, is the shell intersection region.

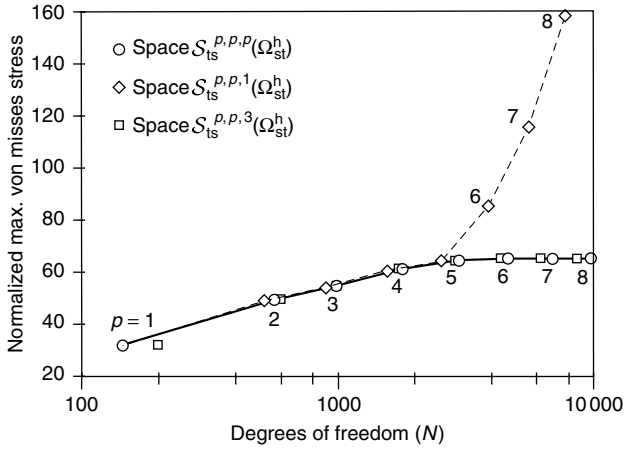

Figure 21. Example: Shell intersection problem. Convergence of the maximum von Mises stress normalized with respect to the applied pressure $\bar{p}$. The estimated limit is 64.7. The maximum occurs in the shell intersection region.

The results are shown in Figure 21. Very strong convergence to the estimated limit value of 64.7 is observed when the isotropic spaces $\mathcal{S}_{\text{ts}}^{p,p,p}(\Omega_{\text{st}}^{\text{h}})$ are employed. This is true also for the anisotropic spaces $\mathcal{S}_{\text{ts}}^{p,p,q}(\Omega_{\text{st}}^{\text{h}})$ for $q \geq 2$ but not for $q = 1$. The reason is that $q = 1$ implies kinematic assumptions similar to those of the Naghdi shell theory. This introduces an artificial singularity along the faces where q changes abruptly from 8 to 1. Essentially, this is a modeling error in the sense it pertains to the question of whether and where a particular shell model is applicable, given that the goal is to approximate some functional of the exact solution of the underlying fully three-dimensional problem. Some aspects of this problem have been addressed in Schwab (1996) and Actis, Szabó and Schwab (1999). This example illustrates the importance of convergence tests on the data of interest, including tests on the choice of dimensionally reduced models.

5 APPLICATIONS TO NONLINEAR PROBLEMS

5.1 Elastoplasticity

The p- and hp-versions of the finite element method have been widely accepted as efficient, accurate, and flexible

methods for analyzing linear problems in computational mechanics. On the other hand, applications of the p- and hp-versions to nonlinear problems are relatively recent and hence less well known. Considering for instance, the J_2 flow theory of elastoplasticity, a loss of regularity is expected along the boundary of the plastic zone. Following the classification of Section 3.1, this problem is of Class C, that is, it has an unknown line (in 2D) or surface (in 3D) of singular behavior in the interior of the domain. Therefore, only an algebraic rate of convergence can be expected. However, this asymptotic rate does not give information on the preasymptotic behavior, that is, on the accuracy of a p-extension for a finite number of degrees of freedom, and especially on the question of computational investment for a desired accuracy of quantities of engineering interest.

To shed some light on this question, we will investigate the deformation theory of plasticity, first proposed by Hencky (1924), as a very simple model problem for elastoplasticity. For a detailed description and numerical investigation of this model problem, see Szabó, Actis and Holzer (1995) and Düster and Rank (2001). We refer to Holzer and Yosibash (1996), Düster and Rank (2002), and Düster *et al.* (2002) for a study of the more complex and physically more realistic flow theory of plasticity, where each load integration step in an incremental analysis can be considered equivalent to the model problem investigated in the following section.

5.1.1 A benchmark problem

As a numerical example, we again use the structure of Figure 9 in Section 2.4.2 showing a quarter of a square plate with central hole and unit thickness, loaded now by a uniform tension of magnitude $T_n = 450$ MPa. The dimensions of the plate are chosen to be $b = h = 10$ mm and the radius is set to $R = 1$ mm. The material is now assumed to be elastic, perfectly plastic and plane strain conditions are assumed. The shear modulus is $\mu = 80193.8$ MPa, the bulk modulus is $\kappa = 164206.0$ MPa, and the yield stress is $\sigma_0 = 450.0$ MPa. This problem was defined by Stein (2002) as a benchmark problem for the German research project 'Adaptive finite-element methods in applied mechanics'.

To find an approximate solution for the given benchmark, we use the p-version based on the tensor product space $\mathcal{S}^{p,p}_{\mathrm{ps}}(\Omega^{\mathrm{q}}_{\mathrm{st}})$ taking advantage of the blending function method. Three different meshes with 2, 4 and 10 p-elements have been chosen (see Figure 22). A series of computations for polynomial degrees $p \leq 17$ for the mesh with 2 elements and $p \leq 9$ for the meshes with 4 and 10 elements was performed. In order to make a comparison with an adaptive h-version, we refer to the results of Barthold, Schmidt and Stein (1997, 1998) and Stein *et al.* (1997). The computations there were performed with the Q1-P0 element differing from the well known bilinear quadrilateral element by including an additional, elementwise constant pressure degree of freedom. A mesh consisting of 64 Q1-P0 elements was refined in 10 steps using the equilibrium criterion, yielding 875 elements with 1816 degrees of freedom (see Figure 23). In Barthold, Schmidt and Stein (1997, 1998) and Stein *et al.* (1997), the results of a sequence of graded meshes and a reference solution obtained with 24 200 Q1-P0 elements with a corresponding number of 49 062 degrees of freedom are also given. Comparing the results of the uniform p-version with those of the h-version based on a sequence of graded meshes, we observe that the efficiency of the p-version is superior (see Figures 24, 25). The discretization with 4 elements, $p = 9$, and 684 degrees of freedom provides an accuracy that cannot be reached by the h-version, even when using 4096 Q1-P0 elements with 8320 degrees of freedom. Even compared to an h-refinement, resulting in an adapted mesh with 875 Q1-P0 elements, it can be seen that a uniform p-version is much more accurate. Although the p-version is significantly more elaborate than the h-version, when comparing the computational effort per degree of freedom, investigations on the computational cost to obtain highly accurate results have clearly shown a superiority of high-order elements. For further information, including three-dimensional examples of the J_2 flow theory with nonlinear isotropic hardening, we refer to Düster and Rank (2001, 2002), Düster (2002), Düster *et al.* (2002), Rank *et al.* (2002), and Stein (2002).

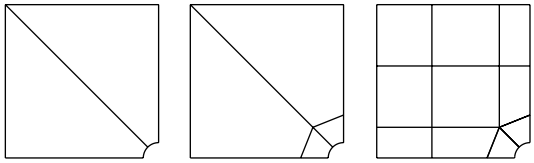

Figure 22. Three meshes with 2, 4, and 10 p-elements. (Reprinted from *Comput. Methods Appl. Mech. Engng.*, **190**, A. Düster and E. Rank, The p-version of the finite-element method is compared to an adaptive h-version for the deformation theory of plasticity, 1925–1935, Copyright (2001), with permission from Elsevier.)

5.1.2 An industrial application

The following example is concerned with a structural component of moderate complexity, called a *dragbrace fitting*, shown in Figure 26. This part is representative of structural components used in the aerospace sector in that relatively thin plate-like regions are reinforced by integrally machined stiffeners. The overall dimensions are length $L = 219.6$ mm and width $w = 115$ mm. The material is typically aluminum or titanium, which exhibit strain hardening. For

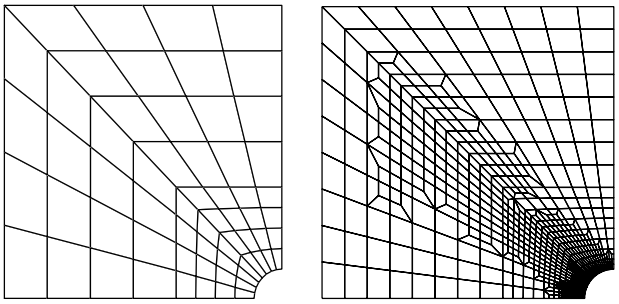

Figure 23. Initial mesh with 64 Q1-P0 elements and adapted mesh with 875 Q1-P0 elements (see Barthold, Schmidt and Stein, 1997). (Reprinted from *Comput. Methods Appl. Mech. Engng.*, **190**, A. Düster and E. Rank, The p-version of the finite-element method compared to an adaptive h-version for the deformation theory of plasticity, 1925–1935, Copyright (2001), with permission from Elsevier.)

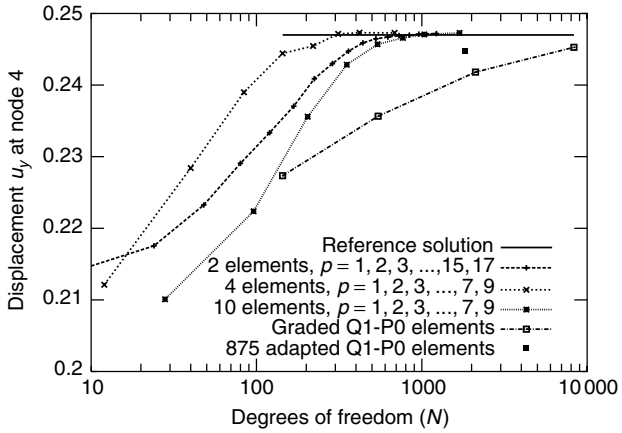

Figure 24. Displacement u_y at node 4. (Reprinted from *Comput. Methods Appl. Mech. Engng.*, **190**, A. Düster and E. Rank, The p-version of the finite-element method compared to an adaptive h-version for the deformation theory of plasticity, 1925–1935, Copyright (2001), with permission from Elsevier.)

the purposes of this example, an elastic–perfectly plastic material was chosen because it poses a more challenging problem from the numerical point of view. The material properties are those of an ASTM A-36 steel; the yield point is 248 MPa, the modulus of elasticity is $E = 200$ GPa, and Poisson's ratio is $\nu = 0.295$. The mathematical model is based on the deformation theory of plasticity.

The lugs A and B are fully constrained and sinusoidally distributed normal tractions are applied through lugs C and D. The resultants of the tractions are F and $2F$ respectively, acting in the negative x direction as the dark region shown schematically in Figure 26. The goal of the computation is to determine the extent of the plastic zone, given that $F = 5.5$ kN. The mesh consists of 2 tetrahedral elements, 22 pentahedral elements, and 182 hexahedral elements.

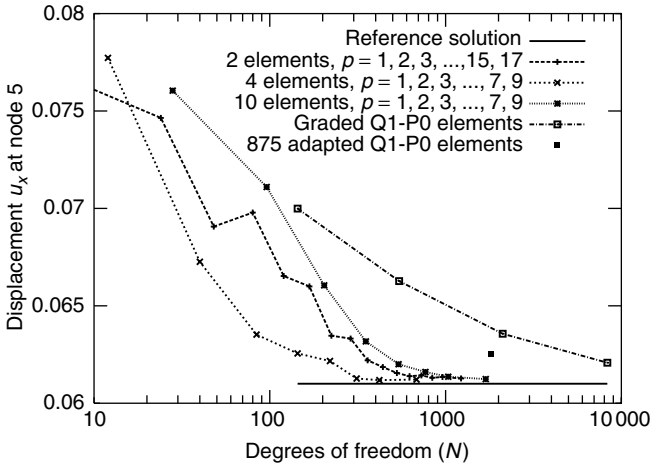

Figure 25. Displacement u_x at node 5. (Reprinted from *Comput. Methods Appl. Mech. Engng.*, **190**, A. Düster and E. Rank, The p-version of the finite-element method compared to an adaptive h-version for the deformation theory of plasticity, 1925–1935, Copyright (2001), with permission from Elsevier.)

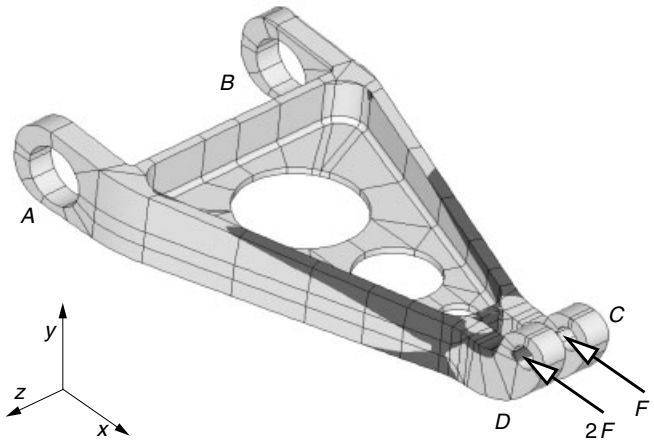

Figure 26. Example: Dragbrace fitting. Elastic-plastic solution, $p = 7$, trunk space, $N = 49\,894$. In the dark region, the equivalent strain exceeds the yield strain.

The region of primary interest is the neighborhood of the loaded lugs. The results of linear analysis indicate that the maximal von Mises stress in this region is 1040 MPa, that is, 4.2 times the yield stress. Therefore, nonlinear analysis has to be performed. The region where the equivalent strain exceeds the yield strain is shown in Figure 26. The computations were performed with StressCheck.

5.2 Geometric nonlinearity

The following example illustrates an application of the p-version to a geometrically nonlinear problem. In geometrically nonlinear problems, equilibrium is satisfied in the

deformed configuration. The constitutive laws establish a relationship either between the Piola–Kirchhoff stress tensor and the Euler–Lagrange strain tensor or the Cauchy stress tensor and the Almansi strain tensor. The formulation in this example is based on the Cauchy stress and the Almansi strain; see Noël and Szabó (1997). The mapping functions given by equation (25) are updated iteratively by the displacement vector components. For example, at the ith iteration, the x-coordinate is mapped by

$$x^{(i)} = Q_x^e(\xi, \eta, \zeta) + u_x^{(i)}(\xi, \eta, \zeta) \tag{49}$$

It is known that when a thin elastic strip is subjected to pure bending, it deforms so that the curvature is constant and proportional to the bending moment:

$$\frac{1}{\rho} = \frac{M}{EI} \tag{50}$$

where ρ is the radius of curvature, M is the bending moment, E is the modulus of elasticity, and I is the moment of inertia. Poisson's ratio ν is zero. In this example, a thin strip of length $L = 100$ mm, thickness $t = 0.5$ mm, and width $b = 5$ mm is subjected to normal tractions on Face A shown in Figure 27, which correspond to M chosen so that $\rho = L/2\pi$:

$$T_n = -\frac{2\pi E}{L}\bar{y} \tag{51}$$

where $\bar{y}$ is measured from the mid surface in the direction of the normal in the current configuration. The three displacement vector components are set to zero on Face B. Three hexahedral elements were used. The anisotropic space $\mathcal{S}_{\text{ts}}^{p,p,1}(\Omega_{\text{st}}^{\text{h}})$ described in Section 2.3 was used. Mapping was by the blending function method using 6×6 collocation points in the quasi-regional mapping procedure described by Királyfalvi and Szabó (1997). The computations were performed with StressCheck. The load T_n was applied in 20 equal increments. The final deformed configuration, a nearly perfect cylindrical body, is shown in Figure 27. The exact solution of a perfectly cylindrical middle surface (the elastica) is the limiting case with respect to the thickness approaching zero.

This example illustrates the following: (a) In the p-version, very large aspect ratios can be used. (b) Quasi-regional mapping, which is an extension of isoparametric mapping combined with the blending function method, is capable of providing a highly accurate representation of the geometrical description with very few elements over large deformations. In this example, Face A was rotated 360 degrees relative to its reference position.

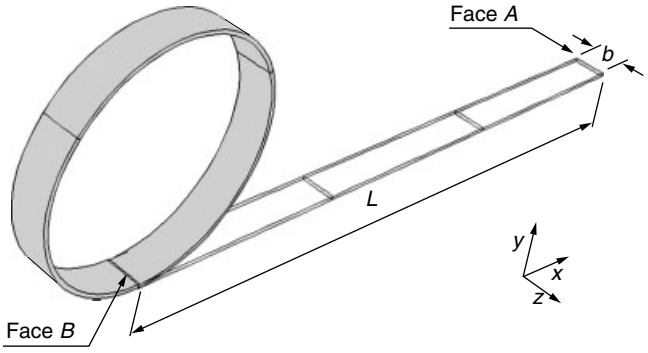

Figure 27. Example: Thin elastic strip. Geometrically nonlinear solution. Three hexahedral elements, anisotropic space $\mathcal{S}_{\text{ts}}^{8,8,1}(\Omega_{\text{st}}^{\text{h}})$, $N = 684$.

6 OUTLOOK

Although implementations of the p-version are available in a number of commercial finite element computer codes, widespread applications of the p-version in professional practice have been limited by three factors:

1. The infrastructure of the most widely used FEA software products was designed for the h-version, and cannot be readily adapted to meet the technical requirements of the p-version.
2. In typical industrial problems, finite element meshes are generated by automatic mesh generators that produce very large numbers of tetrahedral elements mapped by low-order (linear or quadratic) polynomial mapping functions. When the mapping functions are of low degree, the use of high-order elements is generally not justified. This point was illustrated in Section 2.4.2. Nevertheless, numerous computational experiments have shown that p-extension performed on tetrahedral meshes up to $p = 4$ or $p = 5$ provides efficient means of verification for the computed data when the mappings are proper, that is, the Jacobian determinant is positive over every element. Experience has shown that many commercial mesh generators produce improperly mapped elements. As mesh generators improve and produce fewer elements and more accurate mappings, this obstacle will be gradually removed.
3. The demand for verified information in industrial applications of FEMs has been generally weak; however, as computed information is becoming an increasingly important part of the engineering decision-making process, the demand for verified data, and hence the importance of the p-version, is likely to increase.

At present, the p-version is employed in industrial applications mainly where it provides unique technical capabilities. Some examples are: (a) Analysis of mechanical and structural components comprised of plate- and shell-like regions where dimensional reduction is applicable, and solid regions where fully three-dimensional representation is necessary. An example of this kind of domain is shown in Figure 26 where it would not be feasible to employ fully automatic mesh generators because the fillets would cause the creation of an excessive number of tetrahedral elements. On the other hand, if the fillets were omitted, then the stresses could not be determined in the most critical regions. (b) Two- and three-dimensional linear elastic fracture mechanics where p-extensions on geometric meshes, combined with advanced extraction procedures, provide verified data very efficiently; see, for example, Szabó and Babuska (1988) and Andersson, Falk and Babuska (1990). (c) Plate and shell models where the robustness of the p-version and its ability to resolve boundary layer effects are important; see, for example, Babuska, Szabó and Actis (1992), Actis, Szabó and Schwab (1999), and Rank, Krause and Preusch (1998). (d) Analysis of structural components made of composite materials where special care must be exercised in choosing the mathematical model; large aspect ratios must be used and geometric as well as material nonlinear effects may have to be considered; see Engelstad and Actis (2003). (e) Interpretation of experimental data where strict control of the errors of discretization (as well as the experimental errors) is essential for proper interpretation of the results of physical experiments.

The p-version continues to be a subject of research aimed at broadening its application to new areas. Only a few of the many important recent and ongoing research activities can be mentioned here. Application of the p- and hp-versions to mechanical contact is discussed in Páczelt and Szabó (2002) and the references listed therein. The problem of hp-adaptivity was addressed in the papers Demkowicz, Oden and Rachowicz (1989), Oden *et al.* (1989), Rachowicz, Oden and Demkowicz (1989), and Demkowicz, Rachowicz and Devloo (2002). The design of p-adaptive methods for elliptic problems was addressed in Bertóti and Szabó (1998). The problem of combining p- and hp-methods with boundary element methods (BEMs) for the solution of elastic scattering problems is discussed in Demkowicz and Oden (1996). Further information on coupling of FEM and BEM can be found in this encyclopedia (see **Chapter 13, this Volume**). Application of hp-adaptive methods to Maxwell equations was reported in Rachowicz and Demkowicz (2002).

ACKNOWLEDGMENTS

The writers wish to thank Dr Ricardo Actis of Engineering Software Research and Development, Inc., St Louis Missouri, USA for assistance provided in connection with the examples computed with StressCheck and Professor István Páczelt of the University of Miskolc, Hungary, for helpful comments on the manuscript.

NOTES

[1] Waterloo Maple Inc., 57 Erb Street West, Waterloo, Ontarlo, Canada (www.maplesoft.com). The worksheet can be obtained from the Lehrstuhl für Bauinformatik, Technische Universität München, Germany (www.inf.bv.tum.de/∼duester).

[2] StressCheck is a trademark of Engineering Software Research and Development, Inc., St. Louis, Missouri, USA (www.esrd.com).

REFERENCES

Actis Szabó BA and Schwab C. Hierarchic models for laminated plates and shells. *Comput. Methods Appl. Mech. Eng.* 1999; **172**:79–107.

Ainsworth M and Oden JT. *A Posteriori Error Estimation in Finite Element Analysis*. John Wiley & Sons: New York, 2000.

Andersson B, Falk U and Babuška I. *Accurate and Reliable Determination of Edge and Vertex Stress Intensity Factors*. Report FFA TN 1990-28, The Aeronautical Research Institute of Sweden: Stockholm, 1990.

Babuška I and Elman HC. Some aspects of parallel implementation of the finite element method on message passing architectures. *J. Comput. Appl. Math.* 1989; **27**:157–189.

Babuška I and Scapolla T. Computational aspects of the h-, p- and hp-versions of the finite element method. In *Advances in Computer Methods in Partial Differential Equations – VI*, Vichnevetsky R and Stepleman RS (eds). International Association for Mathematics and Computer Simulation (IMACS, 1987; 233–240.

Babuška I and Strouboulis T. *The Finite Element Method and its Reliability*. Oxford University Press: Oxford, 2001.

Babuška I and Suri M. The p- and hp-versions of the finite element method, an overview. *Comput. Methods Appl. Mech. Eng.* 1990; **80**:5–26.

Babuška I and Suri M. On locking and robustness in the finite element method. *SIAM J. Numer. Anal.* 1992; **29**:1261–1293.

Babuška I, Szabó BA and Actis RL. Hierarchic models for laminated composites. *Int. J. Numer. Methods Eng.* 1992; **33**:503–535.

Barthold FJ, Schmidt M and Stein E. Error estimation and mesh adaptivity for elastoplastic deformations. In *Proceedings of*

the 5th International Conference on Computational Plasticity, Complas V, Barcelona, 1997.

Barthold FJ, Schmidt M and Stein E. Error indicators and mesh refinements for finite-element-computations of elastoplastic deformations. *Comput. Mech.* 1998; **22**:225–238.

Bertóti E and Szabó B. Adaptive selection of polynomial degrees on a finite element mesh. *Int. J. Numer. Methods Eng.* 1998; **42**:561–578.

Bröker H. *Integration von geometrischer Modellierung und Berechnung nach der p-Version der FEM*. PhD thesis, Lehrstuhl für Bauinformatik, Technische Universität München, 2001; published in Shaker Verlag: Aachen, ISBN 3-8265-9653-6, 2002.

Chen Q and Babuška I. Approximate optimal points for polynomial interpolation of real functions in an interval and in a triangle. *Comput. Methods Appl. Mech. Eng.* 1995; **128**:405–417.

Chen Q and Babuška I. The optimal symmetrical points for polynomial interpolation of real functions in the tetrahedron. *Comput. Methods Appl. Mech. Eng.* 1996; **137**:89–94.

Demkowicz LF and Oden JT. Application of hp-adaptive BE/FE methods to elastic scattering. *Comput. Methods Appl. Mech. Eng.* 1996; **133**:287–318.

Demkowicz LF, Oden JT and Rachowicz W. Toward a universal h-p adaptive finite element strategy, Part 1. Constrained approximation and data structure. *Comput. Methods Appl. Mech. Eng.* 1989; **77**:79–112.

Demkowicz LF, Rachowicz W and Devloo PH. A fully automatic hp-adaptivity. *J. Sci. Comput.* 2002; **17**:127–155.

Düster A. *High Order Finite Elements for Three-Dimensional, Thin-Walled Nonlinear Continua*. PhD thesis, Lehrstuhl für Bauinformatik, Technische Universität München, 2001; published in Shaker Verlag: Aachen, ISBN 3-8322-0189-0, 2002.

Düster A, Bröker H and Rank E. The p-version of the finite element method for three-dimensional curved thin walled structures. *Int. J. Numer. Methods Eng.* 2001; **52**:673–703.

Düster A, Niggl A, Nübel V and Rank E. A numerical investigation of high-order finite elements for problems of elastoplasticity. *J. Sci. Comput.* 2002; **17**:397–404.

Düster A and Rank E. The p-version of the finite element method compared to an adaptive h-version for the deformation theory of plasticity. *Comput. Methods Appl. Mech. Eng.* 2001; **190**:1925–1935.

Düster A and Rank E. A p-version finite element approach for two- and three-dimensional problems of the J_2 flow theory with non-linear isotropic hardening. *Int. J. Numer. Methods Eng.* 2002; **53**:49–63.

Engelstad SP and Actis RL. Development of p-version handbook solutions for analysis of composite bonded joints. *Comput. Math. Appl.* 2003; **46**:81–94.

Gordon WJ and Hall ChA. Construction of curvilinear co-ordinate systems and applications to mesh generation. *Int. J. Numer. Methods Eng.* 1973a; **7**:461–477.

Gordon WJ and Hall ChA. Transfinite element methods: blending function interpolation over arbitrary curved element domains. *Numer. Math.* 1973b; **21**:109–129.

Grisvard P. *Elliptic Problems in Nonsmooth Domains*. Pitman Advanced Pub. Program: Boston, 1985.

Hencky H. Zur Theorie plastischer Deformationen und der hierdurch im Material hervorgerufenen Nebenspannungen. In *Proceedings of the 1st International Congress on Applied Mechanics*, Delft, 1924.

Holzer S and Yosibash Z. The p-version of the finite element method in incremental elasto-plastic analysis. *Int. J. Numer. Methods Eng.* 1996; **39**:1859–1878.

Királyfalvi G and Szabó BA. Quasi-regional mapping for the p-version of the finite element method. *Finite Elem. Anal. Des.* 1997; **27**:85–97.

Melenk M, Gerdes K and Schwab C. Fully discrete *hp*-finite elements: fast quadrature. *Comput. Methods Appl. Mech. Eng.* 2001; **190**:4339–4369.

Melenk M and Wohlmuth B. On residual-based a-posteriori error estimation in hp-FEM. *Adv. Comput. Math.* 2001; **15**:311–331.

Noël AT and Szabó BA. Formulation of geometrically non-linear problems in the spatial reference frame. *Int. J. Numer. Methods Eng.* 1997; **40**:1263–1280.

Nübel V, Düster A and Rank E. Adaptive vector integration as an efficient quadrature scheme for p-version finite element matrices. In *Proceedings of the European Conference on Computational Mechanics*, Cracow, 2001.

Oden JT, Demkowicz LF, Rachowicz W and Westermann T. Toward a universal h-p adaptive finite element strategy, Part 2. A posteriori error estimation. *Comput. Methods Appl. Mech. Eng.* 1989; **77**:113–180.

Páczelt I and Szabó T. Solution of contact optimization problems of cylindrical bodies using hp-FEM. *Int. J. Numer. Methods Eng.* 2002; **53**:123–146.

Pitkäranta J. The problem of membrane locking in finite element analysis of cylindrical shells. *Numer. Math.* 1992; **61**:523–542.

Rachowicz W, Oden JT and Demkowicz LF. Toward a universal h-p adaptive finite element strategy, Part 3. Design of h-p meshes. *Comput. Methods Appl. Mech. Eng.* 1989; **77**:181–212.

Rachowicz W and Demkowicz LF. An hp-adaptive finite element method for electromagnetics – Part II: A 3D implementation. *Int. J. Numer. Methods Eng.* 2002; **53**:147–180.

Rank E. Adaptive remeshing and h-p domain decomposition. *Comput. Methods Appl. Mech. Eng.* 1992; **101**:299–313.

Rank E and Babuška I. An expert system for the optimal mesh design in the hp-version of the finite element method. *Int. J. Numer. Methods Eng.* 1987; **24**:2087–2106.

Rank E, Bröker H, Düster A, Krause R and Rücker M. The p-version of the finite element method for structural problems. In *Error-controlled Adaptive Finite Elements in Solid Mechanics*, Stein E (ed.). John Wiley & Sons: New York, 2002; 263–307.

Rank E, Krause R and Preusch K. On the accuracy of p-version elements for the Reissner-Mindlin plate problem. *Int. J. Numer. Methods Eng.* 1998; **43**:51–67.

Rank E, Rücker M, Düster A and Bröker H. The efficiency of the p-version finite element method in a distributed computing environment. *Int. J. Numer. Methods Eng.* 2001; **52**:589–604.

Schwab Ch. *p- and hp-Finite Element Methods*. Oxford University Press: Oxford, 1998.

Schwab C. A-posteriori modeling error estimation for hierarchic plate models. *Numer. Math.* 1996; **74**:221–259.

Stein E. *Error-Controlled Adaptive Finite Elements in Solid Mechanics*. John Wiley & Sons, 2002.

Stein E, Barthold FJ, Ohnimus S and Schmidt M. Adaptive finite elements in elastoplasticity with mechanical error indicators and neumann-type estimators. In *Proceedings of the Workshop on New Advances in Adaptive Computational Mechanics*, Cachan, 1997.

Szabó BA, Actis R and Holzer S. Solution of elastic-plastic stress analysis problems by the p-version of the finite element method. In *Modeling, Mesh Generation, and Adaptive Numerical Methods for Partial Differential Equations*, IMA Volumes in Mathematics and its Applications, vol. 75, Babuška I and Flaherty J (eds). Springer, 1995; 395–416.

Szabó BA and Babuška I. Computation of the amplitude of stress singular terms for cracks and reentrant corners. In *Fracture Mechanics: Nineteenth Symposium*, Cruse T (ed.), ASTM STP 969. Philadelphia, 1988; 101–124.

Szabó BA and Babuška I. *Finite Element Analysis*. John Wiley & Sons: New York, 1991.

Szabó BA. The p- and hp-versions of the finite element method in solid mechanics. *Comput. Methods Appl. Mech. Eng.* 1990; **80**:185–195.

Vogelius M. An analysis of the p-version of the finite element method for nearly incompressible materials – uniformly valid optimal estimates. *Numer. Math.* 1983; **41**:39–53.

Yosibash Z and Szabó B. Convergence of stress maxima in finite element computations. *Commun. Numer. Methods Eng.* 1994; **10**:683–697.

FURTHER READING

Simo JC and Hughes TJR. *Computational Inelasticity*. Springer-Verlag: New York, 1998.